Nanocrystal Networks

DOI: 10.1002/anie.201204289

Mesoporous Metal and Metal Alloy Particles Synthesized by Aerosol-Assisted Confined Growth of Nanocrystals**

Qiangfeng Xiao, Hiesang Sohn, Zheng Chen, Daniel Toso, Matthew Mechlenburg, Z. Hong Zhou, Eric Poirier, Anne Dailly, Haiqiang Wang, Zhongbiao Wu, Mei Cai,* and Yunfeng Lu**

Porous materials are broadly used in a diverse range of applications; their unique properties are often influenced significantly by the framework composition.[1–6] To date, various porous materials were synthesized, however, the framework compositions are mainly limited to carbon powders,[4] oxides,[3,5] metal–organic complexes,[7] and polymers.[8] Generally, porous metals hold great promises for a broad spectrum of applications, such as hydrogen storage and catalysis;[1,3,4] however, the porous metals that were reported so far are limited to noble metals, such as Pt,[9] Au,[10] Pd,[11] and Ru.[12] For comparison, the past two decades have witnessed remarkable progress in the synthesis of metal nanocrystals, which were generally obtained by thermal decomposition or reduction reaction of the precursors in the presence of capping ligands.[13,14] Such nanocrystals could be rapidly generated within a confined submicron-size space; their subsequent confined growth gives three-dimensional (3D) nanocrystal networks, the composition of which can be defined through judicious choice of the precursors.

Built on this hypothesis, we report herein a general synthesis of mesoporous metal and metal alloy particles with defined composition using an aerosol approach.[15] We started from non-aqueous solutions (e.g., tetrahydrofuran as solvent) of metal oleates, $M(OA)_x$, in which M is a metal ion and OA is oleic acid (Figure 1).[16] An atomization process with nitrogen as the carrier gas continuously generated precursor droplets. Solvent evaporation from the droplets enriched the precursors and resulted in highly concentrated $M(OA)_x$ aerosol particles (step 1). Subsequent thermal decomposition of the solvent molecules and the precursors (see Figure S1 in the Supporting Information) within the heating zone created an atmosphere that contained reducing molecules (e.g., CO and -CHO; see gas chromatography (GC) analysis in Figure S2)[17] and generated nanocrystals (step 2), which were sequentially grown into nanocrystal clusters and networks (steps 3 and 4). The subsequent sintering process further solidified the networks and removed the organic residuals, thus resulting in the formation of mesoporous particles, the composition of which was controlled through the choice of precursors. It is noteworthy, that various metal oleates are commercially available or can be readily synthesized, ensuring the general applicability of this platform technology. It is also important to point out that, although aerosol processes have been used to synthesize mesoporous oxide particles (e.g., SiO_2),[15] such syntheses were often conducted by using aqueous solvents, thus precluding their use for the synthesis of non-noble metal particles.

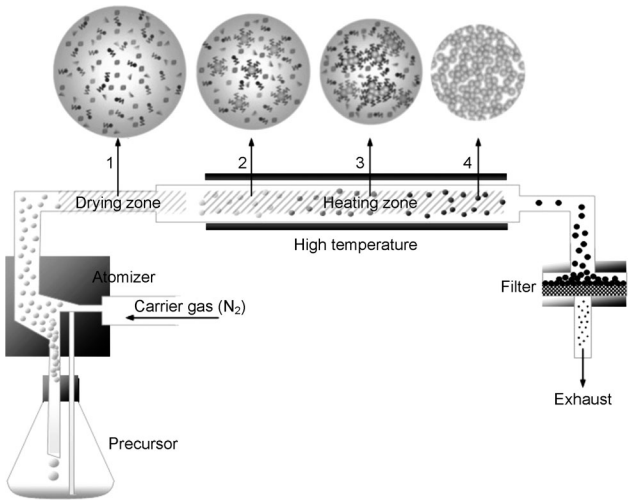

Figure 1. Formation of mesoporous particles through an aerosol-assisted synthesis platform.

[*] Dr. X. F. Xiao,[+] Dr. H. Sohn,[+] Z. Chen, Prof. Y. Lu
Department of Chemical & Biomolecular Engineering
University of California
Los Angeles, CA 90095 (USA)
E-mail: luucla@ucla.edu

Dr. D. Toso, Dr. M. Mechlenburg, Prof. Z. H. Zhou
Department of Microbiology, Immunology & Molecular Genetics;
California NanoSystems Institute
Department of Physics and Astronomy, University of California
Los Angeles, CA 90095 (USA)

Dr. E. Poirier, Dr. A. Dailly, Dr. M. Cai
General Motors Research and Development Center
30500 Mound Road, Warren, MI 48090 (USA)
E-mail: mei.cai@gm.com

Prof. H. Wang, Prof. Z. Wu
Department of Environmental Engineering
Zhejiang University
Hangzhou, 310027 (China)
E-mail: zbwu@zju.edu.cn

[+] These authors contributed equally to the work.

[**] This work was supported as part of the Molecularly Engineered Energy Materials, an Energy Frontier Research Center funded by the U.S. Department of Energy, Office of Science, Office of Basic Energy Sciences under award DE-SC001342. The authors also acknowledge the support from General Motor Inc. and IMRA America Inc.

Supporting information for this article is available on the WWW under http://dx.doi.org/10.1002/anie.201204289.

As a representative, the synthesis of mesoporous Ni particles from $Ni(OA)_2$ is shown in Figure 2. The transmission electron microscopy (TEM) image of the Ni particles shows the mesoporous structure with particle sizes averaging at approximately 200 nm (Figure 2 A-a). The high-resolution

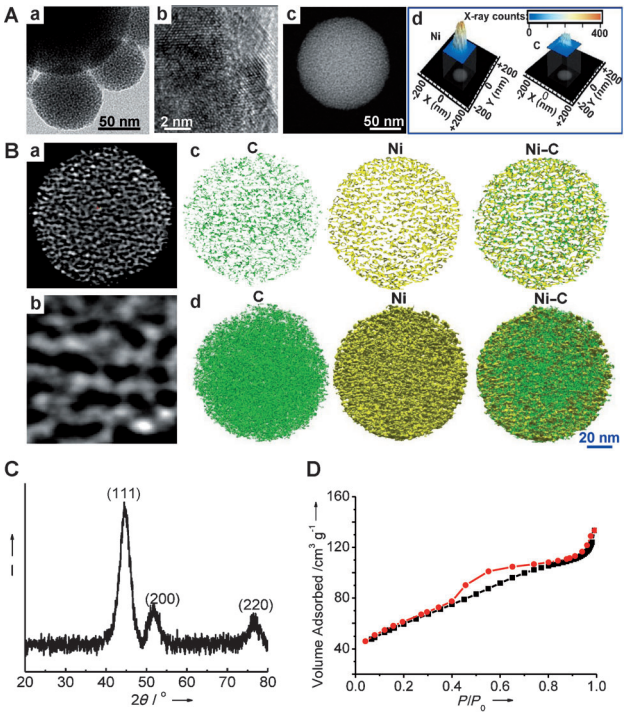

Figure 2. Structure, composition, and morphology of mesoporous Ni particles. A) a) TEM, b) HRTEM, and c) STEM images of mesoporous Ni particles, d) chemical mapping of a representative particle dispersed on a SiO_2-support grid. B) a) Cross-sectional image (3D tomogram) of a Ni particle showing density variation between the Ni framework and surrounding C layer, b) magnified image from (a) further revealing the formation of Ni nanocrystal networks within the particle. c) Cross-sectional mapping images of C (green), Ni (yellow), and their convolution (Ni-C) obtained by the segmentation technique. d) 3D volume reconstruction images of C (green), Ni (yellow), and convoluted 3D networks of Ni and C showing the unique mesoporous architecture. C) XRD patterns and D) N_2 sorption isotherms of Ni particles.

TEM image suggests that these particles are polycrystalline and composed of primary nanocrystals with a diameter of around 3–5 nm (Figure 2 A-b). Their scanning transmission electron microscopy (STEM) image further confirms the mesoporous structure (Figure 2 A-c). The homogeneously distributed black and white spots throughout the particle are identified as Ni and C, respectively, by STEM-EDS chemical mapping analysis (EDS = energy-dispersive X-ray spectroscopy; Figure 2 A-d). The mapping analysis suggests a homogenous distribution of C within the particles. Thermal gravimetric analysis (TGA) indicates that these particles contain approximately 70 and 30 wt % of Ni and C, respectively. X-ray photoelectron spectrum (XPS) suggests that Ni is present in its metallic form, evidenced from the presence of Ni 2p signal and the absence of a NiO signal (Figure S3 c).[18] Consistently, X-ray diffraction (XRD) analysis shows the characteristic (111), (200), and (220) diffractions of the Ni face-centered cubic (FCC) structure (Figure 2 C).[19] Their crystallite are estimated to be 3.4 nm in size by the Scherrer equation, a result that is consistent with TEM observation.

The porous structure was further elucidated through 3D tomographic reconstruction. A cross-sectional image of the tomogram clearly exhibits a uniform spongy skeleton that is composed of Ni nanocrystals and the surrounding C layers (Figure 2 B-a). The magnified image further reveals the spongy structure, which is constructed from the nanocrystal networks (Figure 2 B-b). To further illustrate the structure, total volume reconstruction was further conducted. Cross-section images of a mesoporous particle show the variation of electron density between the nanocrystals (yellow) and the C layers (green; Figure 2 B-c). These elemental sectional images further corroborate homogeneous distribution of Ni and C throughout the particle. Their convoluted image clearly indicates that the fine C grains are uniformly passivated onto the Ni nanocrystals. Figure 2 B-d shows the total volume reconstruction obtained by the combination of the sectional images. Clearly, the mesoporous particles are indeed constructed by networks of Ni nanocrystals, which harmonize with the TEM, STEM, and STEM-EDS results.

Consistent with the structure analysis, nitrogen adsorption–desorption studies (Figure 2 D) provided a type-IV isotherm with a uniform pore diameter averaging at 3.5 nm (Figure S3d). A high surface area of 211 $m^2 g^{-1}$ was achieved, which is much higher than that of the Pt–C nanocomposite with similar metal loading ($\approx$19 $m^2 g^{-1}$, containing 74, 18, 7, and 1 wt % of Pt, C, O and S, respectively).[20] It is also worth mentioning that the surface area contributed by the micropores is approximately 26 $m^2 g^{-1}$, suggesting that most of the surface area is contributed by the mesopores within the particles. Moreover, such a porous structure is highly stable; for example, after sintering in nitrogen at 550 °C for 6.5 h, the particles still retained a surface area larger than 200 $m^2 g^{-1}$ (Figure S4). Similarly, mesoporous particles of Pt, Co, and Fe with high surface area were also synthesized, proving the general applicability of this technology for the synthesis of various mesoporous metals (Figure S5).

Extended from this approach, mesoporous metal alloy particles could also be synthesized by using multiple precursors in a specified ratio. Figure 3 a–c shows representative TEM and STEM images of $Ni_{0.5}Pt_{0.5}$ particles with Ni and Pt oleates in a molar ratio of 1:1. These particles exhibit the mesoporous structure similar to those of the single-metal mesoporous particles; a nitrogen sorption study showed similar isotherms with a high surface area of approximately 143 $m^2 g^{-1}$ (Figure S6b). The TEM image also exhibits a polycrystalline structure, thus indicating that the alloy particles are also composed of primary nanocrystals (Figure 3 b). To further illustrate their structure, EDS (Figure S6a) and chemical mapping (Figure S6c) were conducted on the particles and the results suggest a homogeneous distribution of Ni and Pt throughout the spheres.

The composition of the alloyed particles can be readily tuned by the precursor ratio. For example, Figure 3 d shows XRD patterns of a series of Ni_xPt_{1-x} particles prepared from

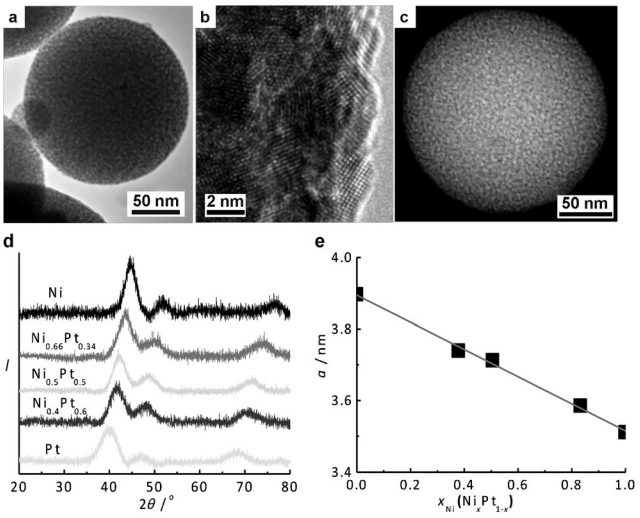

Figure 3. Structure of mesoporous alloy particles. a) TEM, b) HRTEM, and c) STEM images of representative $Ni_{0.5}Pt_{0.5}$ alloyed particles showing mesoporous polycrystalline structure. d) XRD of Ni_xPt_{1-x} with various compositions. e) Linear relationship between the lattice parameter of the alloys versus their Ni content.

mixtures of $Ni(OA)_2$ and $Pt(OA)_4$ with different molar ratios. All samples exhibit an FCC structure with characteristic (111), (200), and (220) diffractions, which systematically shift to the lower 2θ with increasing Pt content, thus indicating the formation of substitution-type alloys formed by replacing Ni with Pt.[21] A linear correlation complying with the Vegard's law, $a = a_{Ni}x + a_{Pt}$-$(1-x)$, in which a_{Ni} and a_{Pt} is the unit cell parameter of Ni or Pt and x is the molar fraction of Ni, further confirms the formation of alloy with tunable composition.[22] It is important to point out that mesoporous particles of binary Ni_xPd_{1-x} alloys and ternary $Ni_xPt_yPd_{1-x-y}$ alloys were also synthesized with tunable composition, further demonstrating the general applicability of this approach (Figure S7).

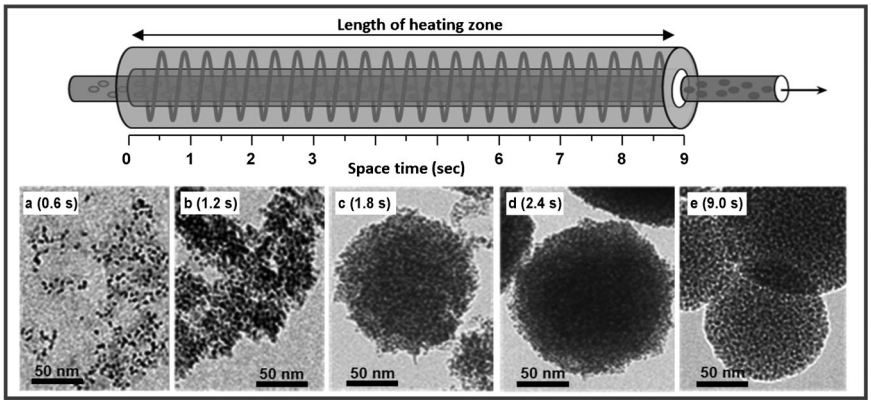

Figure 4. Structural evolution of the mesoporous particles during the continuous aerosol-assisted formation process. TEM images of the samples collected at space time of a) 0.6 s, b) 1.2 s, c) 1.8 s, d) 2.4 s, and e) 9.0 s, respectively, exhibiting structural evolution from nanocrystals to nanocrystal clusters to nanocrystal networks.

The formation of such particles was achieved through such a rapid and continuous process. The average resident time (space time) of the aerosol particles within the heating zone (reacting zone) is estimated to be 9 s, based on the operation condition and the dimension of the tubular reactor (Figure S8). To dissect such a continuous process, we systematically varied the length of the heating-zone and examined the structure of the corresponding particles that were formed. By converting the heating-zone length into the resident time (reaction time), structural evolution of the particles during this continuous process could be readily probed. Figure 4 a–e shows the TEM images of the particles collected with heating-zone lengths corresponding to a space time of 0.6, 1.2, 1.8, 2.4, and 9.0 s, respectively. The sample collected at 0.6 s shows the formation of Ni nanocrystals with a diameter of approximately 3–4 nm, which is consistent with the sizes of the nanocrystals observed in the final porous particles. The sample collected at 1.2 s shows the formation of nanocrystal clusters, which sequentially grew into networks of nanocrystals in 1.8 s. The network structure was further developed and completed with time, evidenced from the samples collected at 2.4 and 9.0 s. Such structure evolution confirms extremely fast reaction kinetics; mesoporous particles were formed continuously in a matter of seconds.

Generally, the composition of the particles is determined by the precursors that are used. Nevertheless, for the synthesis of mesoporous metals, the precursors that are used (metal oleates) contain oxygen moieties, which may lead to the formation of mesoporous oxides rather than metals. Therefore, the composition of the particles would be determined by reaction temperature and intrinsic parameters of the metal moieties, such as Gibbs formation energy of metal oxides ($\Delta G°$) and electronegativity (χ_p).

$\Delta G°$ may be generally described by a three-term equation, $\Delta G° = A + B\,T + C\,T\,logT$, in which T is the temperature and A, B, and C are coefficients that depend on the temperature and the metal.[23] Figure 5 shows plots of $\Delta G°$ for various metals at 550 °C (the temperature used for the synthesis), as well as χ. Considering $\Delta G°$ of CO ($-184.5\ kJ\,mol^{-1}e$) or CO_2 ($-395.6\ kJ\,mol^{-1}e$) from oxidizing the reducing agents (e.g., X, CO, and -CHO), the formation of mesoporous metal particles is thermodynamically favored when $\Delta G°$ is larger than $-395.6\ kJ\,mol^{-1}e$. In our system, the use of Pt, Pd, Cu, and Ni oleates led to the formation of mesoporous metal particles with $\Delta G°$ greater than $-149.3\ kJ\,mol^{-1}$. For metals with a medium range of $\Delta G°$, such as FeO ($-210.5\ kJ\,mol^{-1}$), the product consists of a dominant oxide phase with a small fraction of metallic Fe. When $\Delta G°$ is more negative, such as for ZnO ($-257.5\ kJ\,mol^{-1}$) and MnO ($-331.4\ kJ\,mol^{-1}$), use of the corresponding oleates leads to the formation of mesoporous oxide particles. Since χ_p is a measure of the

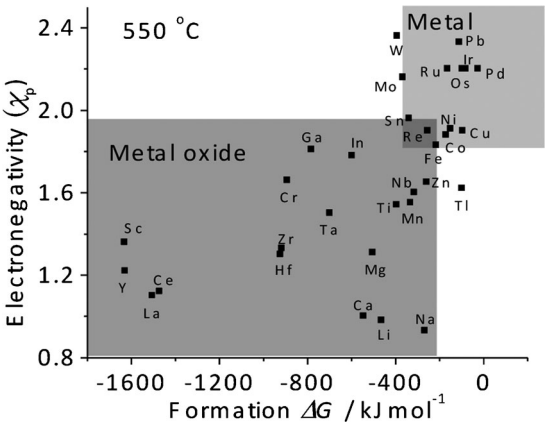

Figure 5. Composition dependence of the mesoporous particles versus the metallic moieties of the precursors. Estimated $\Delta G°$ at 550 °C, plotted against Pauling electronegativity (χ_p) of the corresponding metals.

ability of chemically bonded atoms to attract electrons, the underlying chemistry is more intimately related to χ_p.[24] It was found that metal oleates in which the metal moieties possess $\chi_p \geq 1.90$ (Cu) tend to form mesoporous metals and metal alloys, whereas those with lower χ_p form oxides. Such results provide a roadmap to design porous materials with defined composition (Figure S9–S15).

The capability to synthesize such mesoporous metal particles offers access to unique materials for broad applications. In Figure S16A, a comparison of H_2 uptake at 25 °C for the mesoporous Ni particles, Vulcan XC-72 (a carbon powder with a surface area of 230 $m^2 g^{-1}$), and Ni nanoparticles (30–50 nm in diameter) is given. The mesoporous Ni particles exhibit a H_2 uptake of 0.40 wt % at 80 bar, while other samples only show negligible H_2 uptakes of approximately 10^{-3} wt %. Such results are also comparable to those of Ni-decorated high-surface-area activated carbon powder.[25] Note that extremely high pressure (6.5×10^3 bar) is needed for large Ni particles to reach a similar H_2 uptake.[26] A linear increase of hydrogen storage with pressure is observed in the high-pressure range. Such phenomena are similar to those observed for metal-doped metal–organic frameworks (MOFs) or carbon powder rather than for the metal–hydrogen systems, a result that can be attributed to the presence of a large number of hydrogen binding and dissociation sites, as well as the nanocrystalline network structure that promotes the formation of nickel hydride.[27]

The hydrogen storage capability can be further improved by impregnating MgH_2 within the mesoporous Ni particles. This was achieved by immersion of the particles within dibutylmagnesium heptane solution, followed by treatment at 200 °C under 50 bar H_2.[28] Note that MgH_2 exhibits high storage capacity (7.6 wt %), but sluggish kinetics below 300 °C,[29] which can be improved by incorporating transition metals, such as Ni, Cu, and Pt. Accordingly, Figure S16-B shows hydrogen absorption (normalized to MgH_2 mass) of the mesoporous Ni particles containing 40 wt % of MgH_2 after being desorbed at 250 °C under vacuum before absorption. Impressively, the Mg in the composites starts to absorb hydrogen at 25 °C, while no H_2 absorption is observed for pure MgH_2 below 200 °C. The saturation capacity increases with temperature, reaching 6.2 wt % at 62 bar and 250 °C; while bulk Mg requires 400 °C to reach comparable performance.

In summary, we have developed a platform technology that enables the rapid and continuous synthesis of mesoporous metal and metal alloy particles through confined growth of nanocrystals. Considering the vast library of organometallic precursors that are available, huge families of mesoporous materials with compositions ranging from metals to alloys to oxides may be readily prepared for a broad spectrum of applications.

Experimental Section

Mesoporous particles of metals and alloys were synthesized from metal oleates or their mixtures with specified ratios. The metal oleates are commercially available or were prepared by reacting metal salts or oxides with oleic acid. The precursors were dissolved in organic solvent (e.g., THF and toluene) at a specified ratio and concentration to form homogenous clear solutions. The precursor solutions were atomized by using a commercial pneumatic atomizer (Model 3076, TSI, Inc.) with nitrogen as a carrier/atomization gas. The aerosols passed through a tubular reactor (heated at 550 °C) and converted to the mesoporous particles, which were subsequently collected by the filter. The aerosol reactor is operated at a volumetric flow rate of 2.6 L min^{-1} (STP). The geometry of the tubular reactor within the heating zone is 1″ (ID) × 30″ (L). Synthesized particles were afterwards treated at 550 °C under N_2 atmosphere for 30 min. Details of the chemicals that were used, precursor synthesis, and characterizations are provided in the Supporting Information.

Received: June 2, 2012
Revised: July 26, 2012
Published online: September 23, 2012

Keywords: hydrogen storage · mesoporous materials · nanocrystal networks · nanoparticles · alloys

[1] Y. F. Lu, *Angew. Chem.* **2006**, *118*, 7826–7829; *Angew. Chem. Int. Ed.* **2006**, *45*, 7664–7667.
[2] F. Jiao, J.-C. Jumas, M. Womes, A. V. Chadwick, A. Harrison, P. G. Bruce, *J. Am. Chem. Soc.* **2006**, *128*, 12905–12909.
[3] F. Schüth, *Chem. Mater.* **2001**, *13*, 3184–3195.
[4] C. D. Liang, Z. J. Li, S. Dai, *Angew. Chem.* **2008**, *120*, 3754–3776; *Angew. Chem. Int. Ed.* **2008**, *47*, 3696–3717.
[5] J. Y. Ying, C. P. Mehnert, M. S. Wong, *Angew. Chem.* **1999**, *111*, 58–82; *Angew. Chem. Int. Ed.* **1999**, *38*, 56–77.
[6] Y. S. Tao, H. Kanoh, L. Abrams, K. Kaneko, *Chem. Rev.* **2006**, *106*, 896–910.
[7] N. L. Rosi, M. Eddaoudi, D. T. Vodak, J. Eckert, M. O'Keeffe, O. M. Yaghi, *Science* **2003**, *300*, 1127–1129.
[8] X. Li, S. Tian, Y. Ping, D. H. Kim, W. Knoll, *Langmuir* **2005**, *21*, 9393–9397.
[9] G. S. Attard, P. N. Bartlett, N. R. B. Coleman, J. M. Elliott, J. R. Owen, J. H. Wang, *Science* **1997**, *278*, 838–840.
[10] J. Erlebacher, M. J. Aziz, A. Karma, N. Dimitrov, K. Sieradzk, *Nature* **2001**, *410*, 450–453.
[11] D. H. Wang, H. M. Luo, R. Kou, M. P. Gil, S. G. Xiao, V. O. Golub, Z. Z. Yang, C. J. Brinker, Y. F. Lu, *Angew. Chem.* **2004**, *116*, 6295–6299; *Angew. Chem. Int. Ed.* **2004**, *43*, 6169–6173.
[12] Y. Yamauchi, K. Kuroda, *Chem. Asian J.* **2008**, *3*, 664–676.
[13] S. G. Kwon, T. Hyeon, *Acc. Chem. Res.* **2008**, *41*, 1696–1709.

[14] A. R. Tao, S. Habas, P. D. Yang, *Small* **2008**, *4*, 310 – 325.
[15] Y. F. Lu, H. Y. Fan, A. Stump, T. L. Ward, T. Rieker, C. J. Brinker, *Nature* **1999**, *398*, 223 – 226.
[16] N. R. Jana, Y. F. Chen, X. G. Peng, *Chem. Mater.* **2004**, *16*, 3931 – 3935.
[17] S. G. Kwon, Y. Piao, J. Park, S. Angappane, Y. Jo, N.-M. Hwang, J.-G. Park, T. Hyeon, *J. Am. Chem. Soc.* **2007**, *129*, 12571 – 12584.
[18] A. P. Grosvenor, M. C. Biesinger, R. S. Smart, N. S. McIntyre, *Surf. Sci.* **2006**, *600*, 1771 – 1779.
[19] Y. T. Jeon, J. Y. Moon, G. H. Lee, J. Park, Y. Chang, *J. Phys. Chem. B* **2006**, *110*, 1187 – 1191.
[20] S. C. Warren, L. C. Messina, L. S. Slaughter, M. Kamperman, Q. Zhou, S. M. Gruner, F. J. DiSalvo, U. Wiesner, *Science* **2008**, *320*, 1748 – 1752.
[21] Y. Li, X. L. Zhang, R. Qiu, R. Qiao, Y. S. Kang, *J. Phys. Chem. C* **2007**, *111*, 10747 – 10750.
[22] D. C. Pan, D. Weng, X. L. Wang, Q. F. Xiao, W. Chen, C. L. Xu, Z. Z. Yang, Y. F. Lu, *Chem. Commun.* **2009**, 4221 – 4223.
[23] *CRC Handbook of Chemistry and Physics*, 76th ed., CRC, Boca Raton, FL, **1995**.
[24] D. S. Wang, Q. Peng, Y. D. Li, *Nano Res.* **2010**, *3*, 574 – 580.
[25] L. F. Wang, R. T. Yang, *J. Phys. Chem. C* **2008**, *112*, 12486 – 12494.
[26] B. Baranowski, *Top. Appl. Phys.* **1978**, *29*, 157 – 200.
[27] V. Bérubé, G. Radtke, M. Dresselhaus, G. Chen, *Int. J. Energy Res.* **2007**, *31*, 637 – 663.
[28] T. K. Nielsen, K. Manickam, M. Hirscher, F. Besenbacher, T. R. Jensen, *ACS Nano* **2009**, *3*, 3521 – 3528.
[29] K. J. Jeon, H. R. Moon, A. M. Ruminski, B. Jiang, C. Kisielowski, R. Bardhan, J. J. Urban, *Nat. Mater.* **2011**, *10*, 286 – 290.

